Supplementary Information

Effect of chiral camphor thiolate ligands on the structure and stability of Au_{19} nanoclusters

Xiaoya Zhang,[a] Shuwen Wu,[a] Qinzhen Li,[a] Jinsong Chai,[a] Guiqi Gao,*[a] Baoyu Huang,*[b] Sha Yang*[a] and Manzhou Zhu[a]

[a]Regulation of Hybrid Materials of Ministry of Education, Department of Chemistry and Anhui Province Key Laboratory of Chemistry for Inorganic/Organic Hybrid Functionalized Materials, Anhui University, Hefei, Anhui230601, China.

[b]Department Hunan Provincial Key Laboratory of Environmental Catalysis & Waste Recycling, College of Materials and Chemical Engineering, Hunan Institute of Engineering, 411104 Xiangtan, China.

* Corresponding author. E-mail address: yangshac@ahu.edu.cn; gaoguiqi1@126.com; 22164@hnie.edu.cn

Au_{19} Stability test

Acidity and oxidation stability test

CH_3COOH and tert-Butyl hydroperoxide solution (tbhp) were selected as acids and oxidants respectively. The 1 mg S-Au_{19} cluster was dissolved in 3 mL toluene, and the initial UV-vis and CD spectra were recorded.

Subsequently, 60 uL 1 M acetic acid solution was added to the toluene solution of the clusters. The instability of S-Au_{19} under acidic condition was determined by UV-vis and CD spectroscopy (Fig. S11a and S11b). At 10 min, the characteristic peaks of UV-vis and CD were reduced. The characteristic peaks of UV-vis and CD continued to weaken until 24 h. Although there was a weak trend, the clusters were destroyed in the acidic environment. In addition, tbhp (60 uL) was used to replace acetic acid, and the stability test was carried out in the oxidizing environment. It was found that the characteristic peaks of UV-vis and CD almost disappeared at 6h, and the clusters completely broke down at 9 h, so the clusters are unstable in the oxidizing environment (Fig. S11c and S11d). R-Au_{19} is also unstable in acidic and oxidizing environments (Fig. S12).

UV light stability test

Under UV light condition, the UV-vis characteristic peaks of R/S-Au_{19} began to weaken at 3 h, and became weaker and weaker with time. At 14 h, the UV-vis characteristic peaks disappeared. The clusters were completely destroyed, hence, R/S-Au_{19} are unstable under UV light condition (Fig. S10b and 10d).

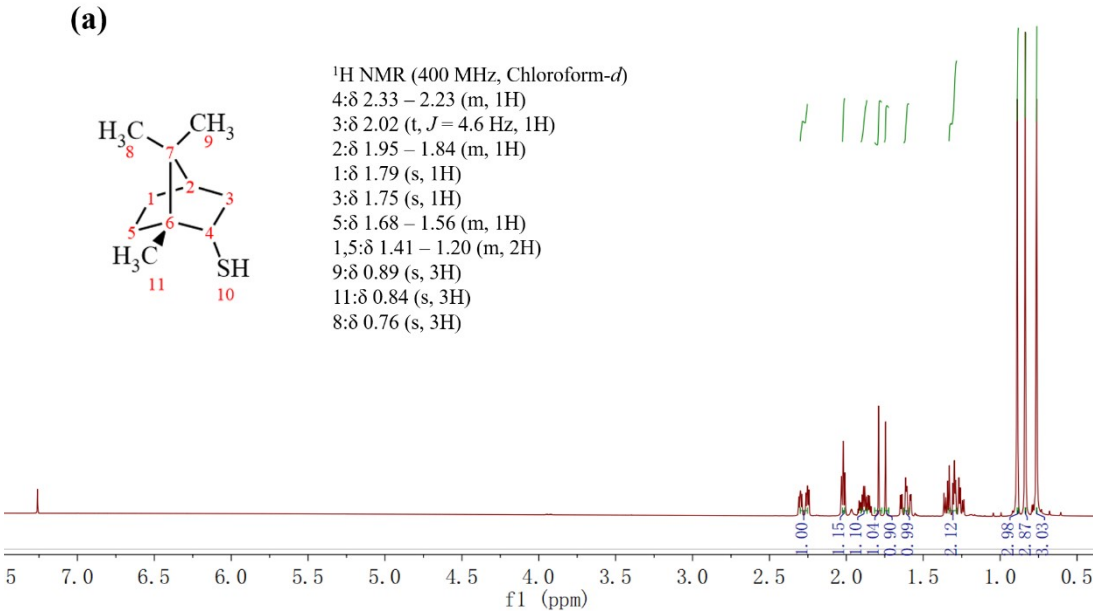

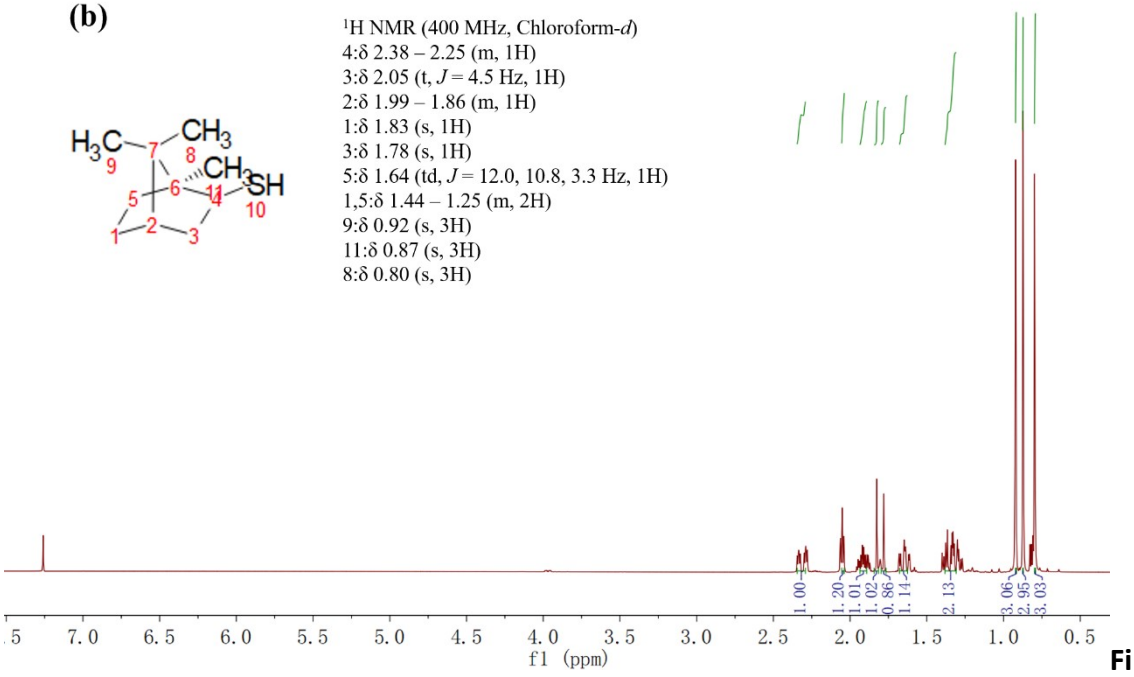

Fig. S1 ^{1}H NMR spectra of (+)-camphor thiol (a) and (−)-camphor thiol (b) in $CDCl_3$.

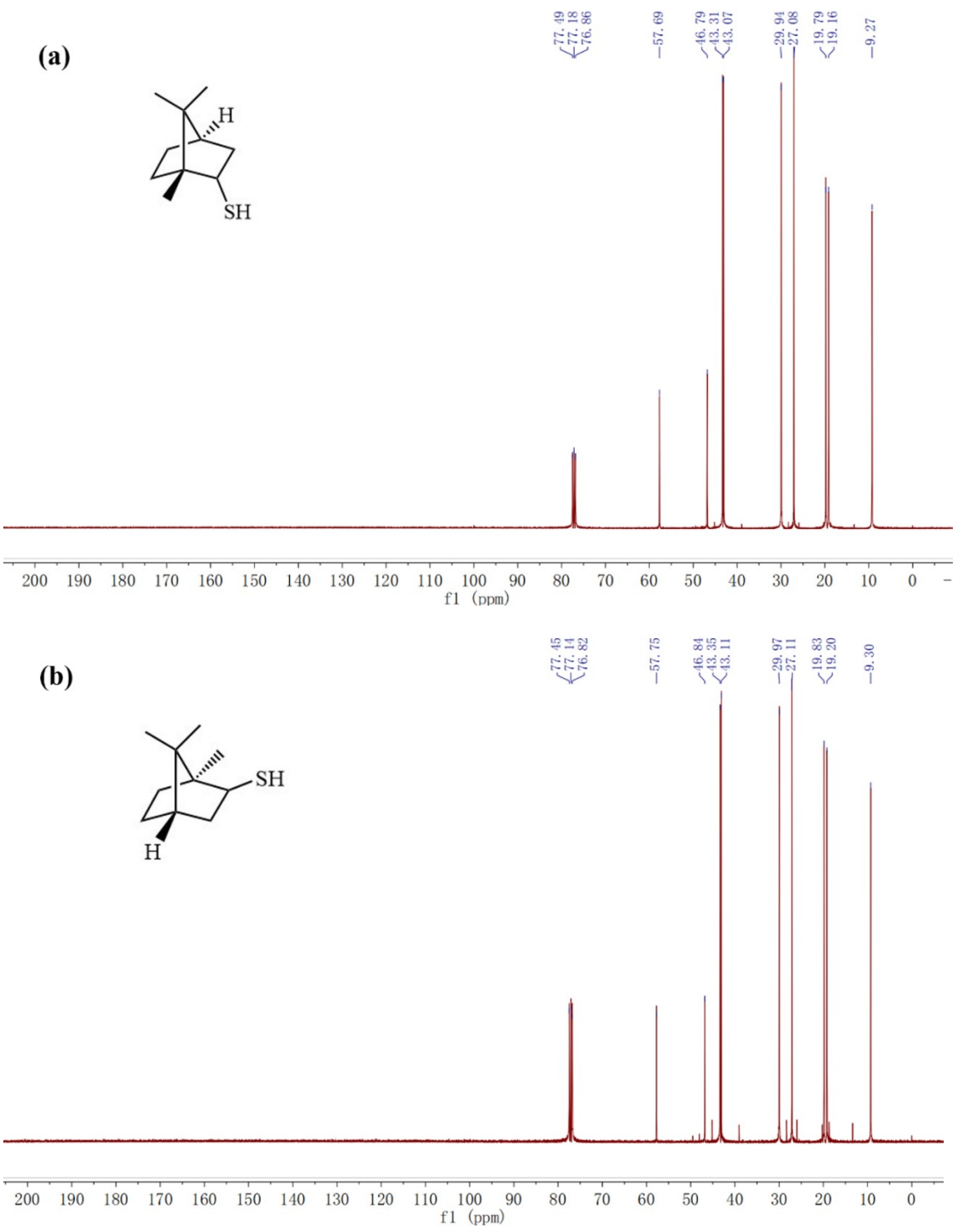

Fig. S2 ^{13}C NMR spectra of (+)-camphor thiol (a) and (−)-camphor thiol (b) (in $CDCl_3$). ^{13}C NMR (101 MHz, Chloroform-d) δ 57.69, 46.79, 43.31, 43.07, 29.94, 27.08, 19.79, 19.16, 9.27 (a); ^{13}C NMR (101 MHz, Chloroform-d) δ 57.75, 46.84, 43.35, 43.11, 29.97, 27.11, 19.83, 19.20, 9.30 (b).

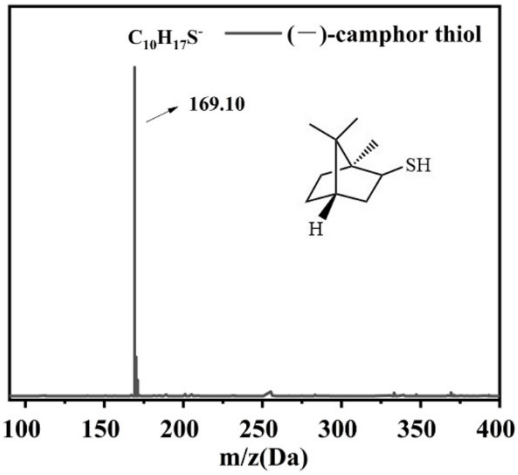

Fig. S3 Electrospray ionization mass spectra of (−)-camphor thiol.

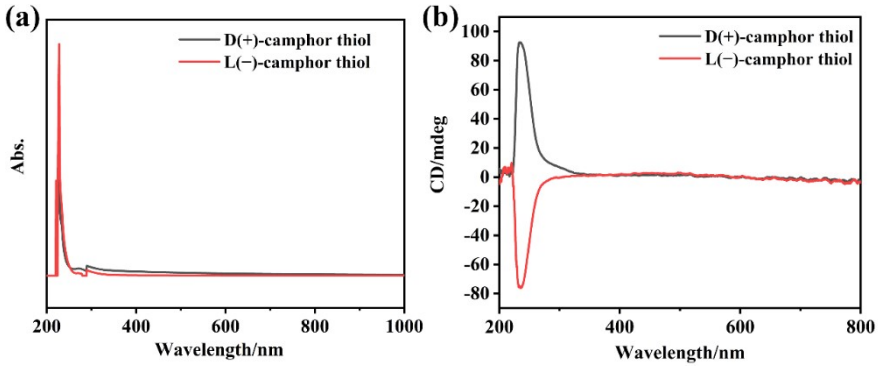

Fig. S4 (a) UV-vis spectra and (b) CD spectra of (+/−)-camphor thiols.

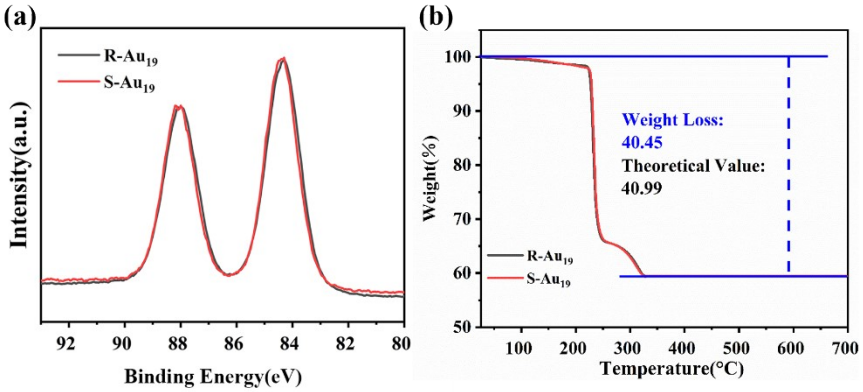

Fig. S5 (a) Au 4f spectra of R/S-Au_{19} and (b)TGA curve of R/S-Au_{19}.

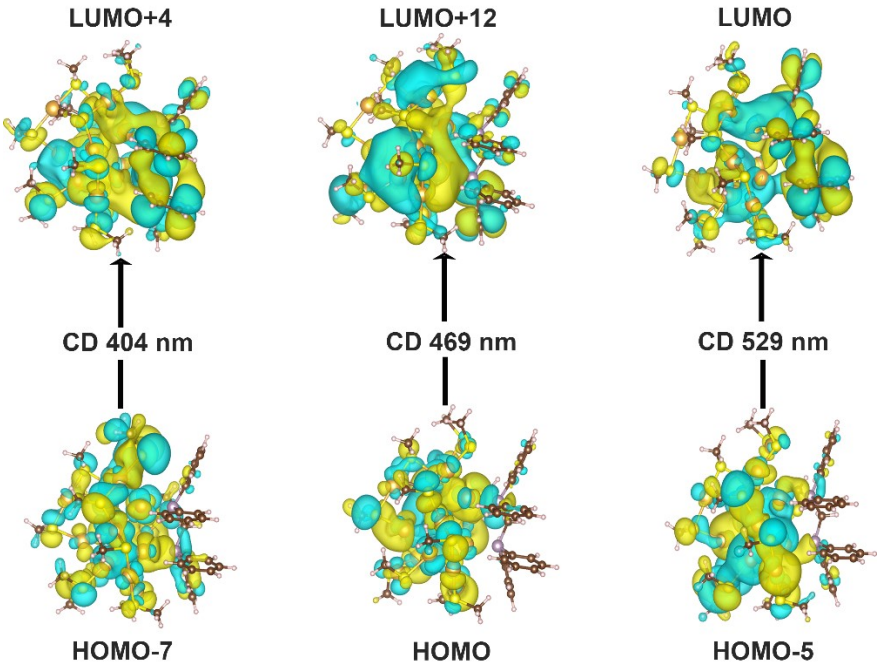

Fig. S6 The calculated HOMO-7 to LUMO+4, HOMO to LUMO+12 and HOMO-5 to LUMO orbitals.

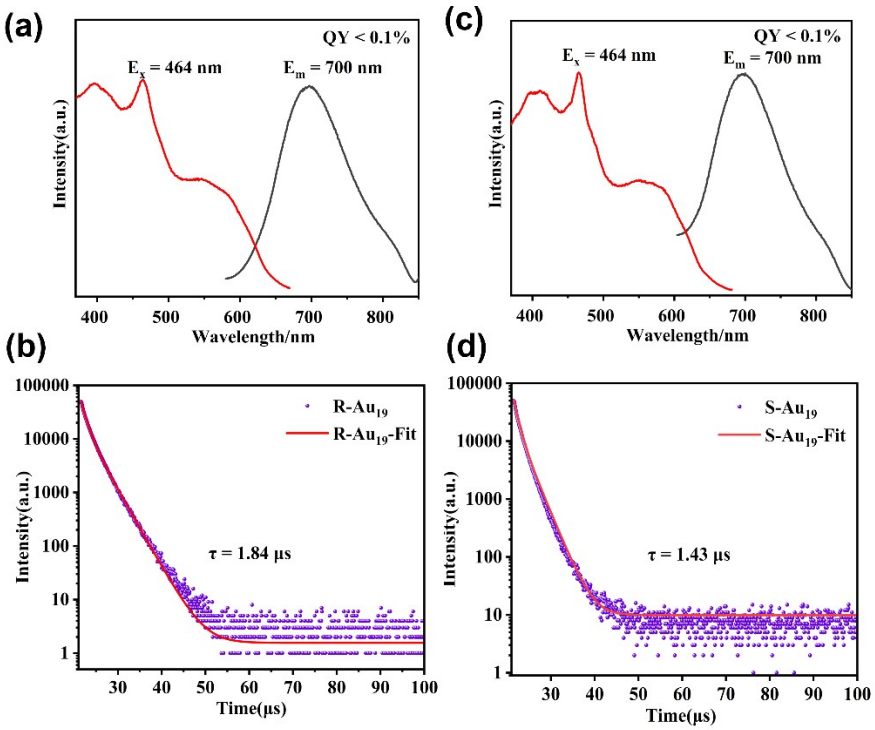

Fig. S7 Photoluminescent excitation and emission spectra of R-Au_{19} (a) and S-Au_{19}(c). Fluorescence lifetime of R-Au_{19} (b) and S-Au_{19} (d).

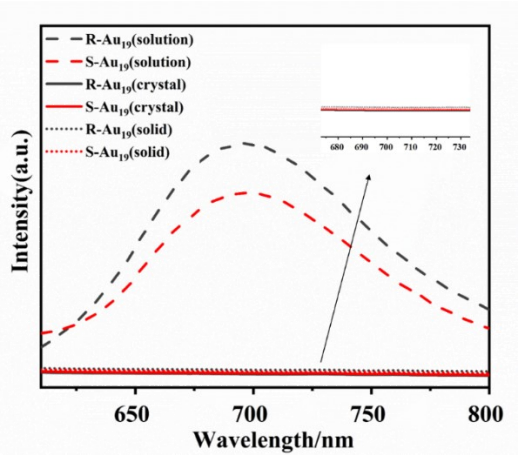

Fig. S8 Comparison of photoluminescence intensity between R/S-Au_{19} crystal, solid, and solution states.

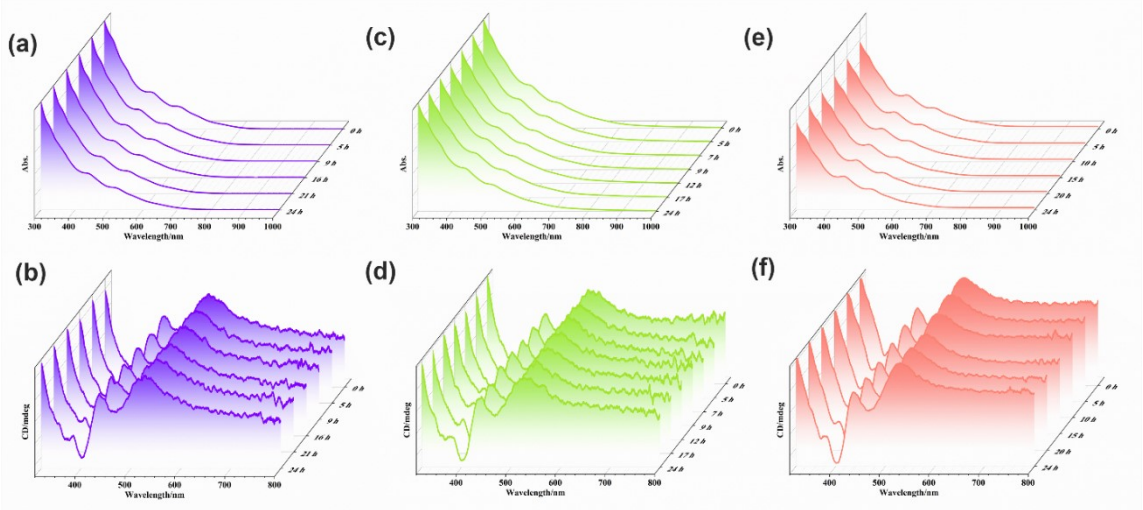

Fig. S9 The time-dependent UV-vis spectra (a) and CD spectra (b) for alkalinity stability test of the S-Au_{19}.The time-dependent UV-vis spectra(c) and CD spectra (d) for reducibility stability test of the S-Au_{19}. The time-dependent UV-vis spectra (e) and CD spectra (f) for thermal stability test of the S-Au_{19} at 60 °C.

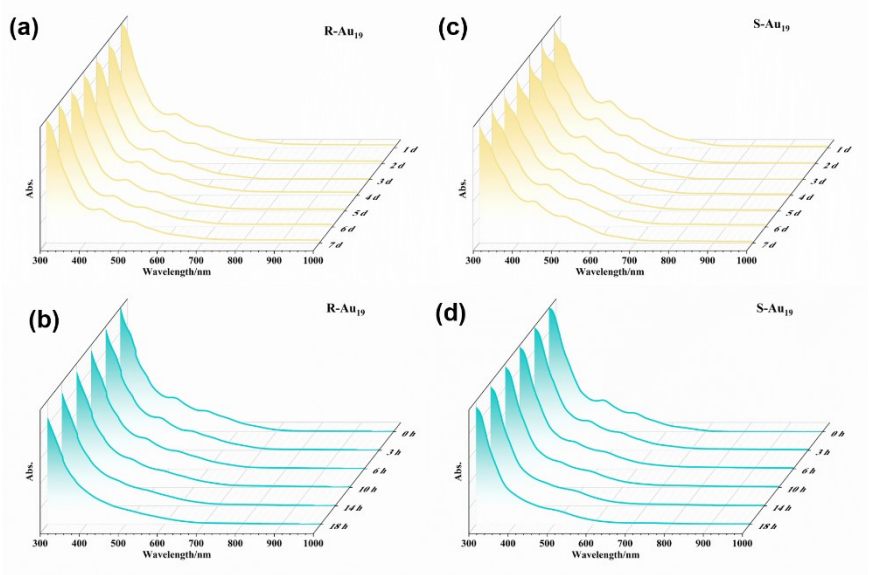

Fig. S10 Time-dependent UV-vis spectra of R-Au_{19} in daylight (a) and UV light (b) stability tests. Time-dependent UV-vis spectra of S-Au_{19} in daylight (c) and UV light (d) stability tests.

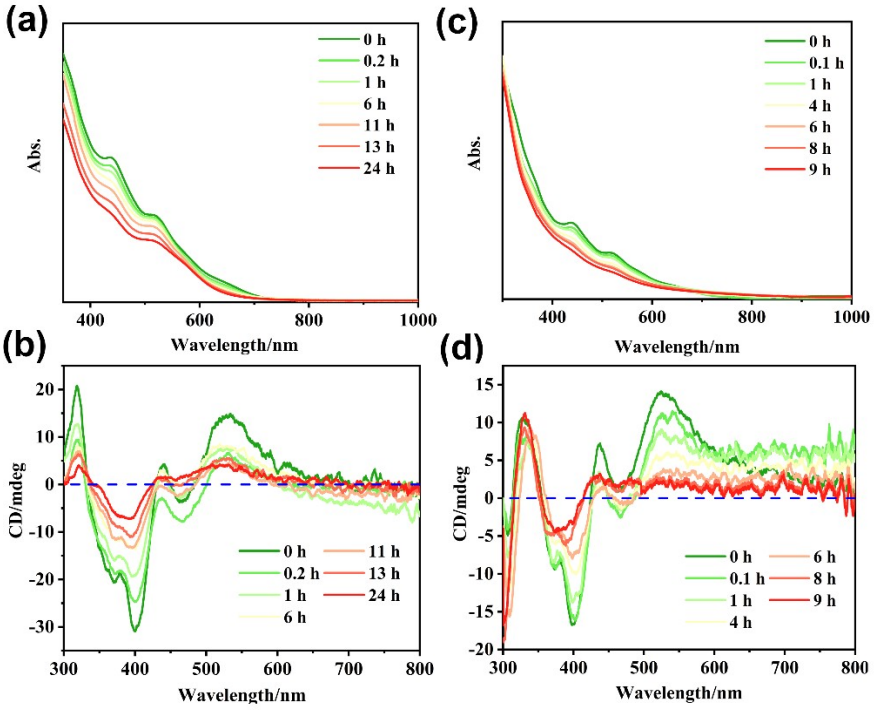

Fig. S11 The time-dependent UV-vis spectra (a) and CD spectra (b) for acidity stability test of the S-Au_{19}. The time-dependent UV-vis spectra (c) and CD spectra (d) for oxidation stability test of the S-Au_{19}.

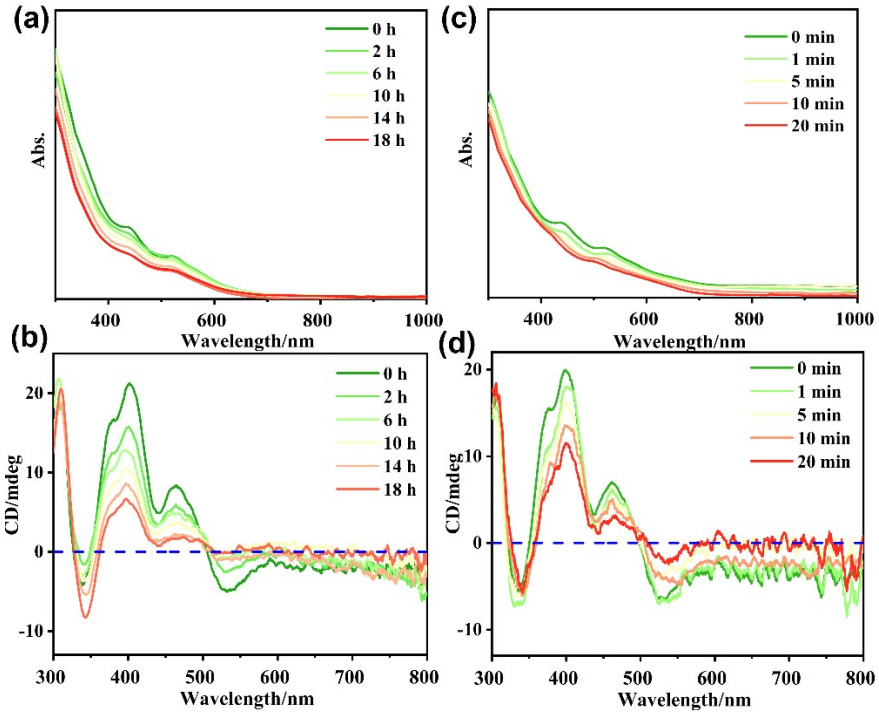

Fig. S12 The time-dependent UV-vis spectra (a) and CD spectra (b) for acidity stability test of the R-Au_{19}. The time-dependent UV-vis spectra (c) and CD spectra (d) for oxidation stability test of the R-Au_{19}.

Table S1 Summarizes of the maximum anisotropy factors of partially reported chair nanoclusters.

NCs	Maximum Anisotropy factors	NCs	Maximum Anisotropy factors
$Au_{19}(SR)_{13}DPPM$	1.89×10^{-3} (this work)	$[Au_{11}(BINAP)_4X_2]^+$	1.2×10^{-3}(12)
$[Au_{13}Cu_2(R/S\text{-}BDPP)_3(SPy)_6]^+$	1.2×10^{-3} (1)	$[Au_{24}L_6Cl_4]^{2+}$	3×10^{-3}(13)
$[Ag_{28}Cu_{12}(SR)_{24}]^{4-}$	1.0×10^{-3} (2)	$Ag_{29}(R/S\text{-}DHLA)_{12}$	1.3×10^{-3}(14)
$[Au_{13}L_5Cl_2]Cl_3$	1.6×10^{-3} (3)	$[Au_{19}(R/S\text{-}BINAP)_4(PhC{\equiv}C)Cl_4]$	1.2×10^{-3}(15)
$[Ag_{47}L_{12}(C{\equiv}C^tBu)_{16}]BF_4$	1.4×10^{-3} (4)	$[Au_{11}(R/S\text{-}BINAP)_4(PhC{\equiv}C)_2]\cdot Cl$	1.2×10^{-3}(15)
$[Au_7Ag_6Cu_2(BINAP)_3(SCH_2Ph)_6]^+$	5×10^{-4} (5)	$Au_{24}(L)_2(SC_6H_{11})_{16}$	0.75×10^{-3}(16)
Ag_{40}	1.6×10^{-3} (6)	$Au_{25}[(Capt)_{18}]^-$	4×10^{-4}(17)
$Au_{24}Cd_2(SAdm)_{12}(BDPP)_2Cl_2$	1.2×10^{-4} (7)	$Au_{38}(SG)_{24}$	1.08×10^{-3}(18)
$Au_{10}(R/S\text{-}BINAP)_4$	6.6×10^{-3}(8)	$Au_{38}(Capt)_{24}$	4×10^{-3}(18)
$Au_9(R/S\text{-}BINAP)_4$	3.7×10^{-3}(8)	$Au_{38}(2\text{-}PET)_{24-x}(CamS)_x$	7×10^{-5}(19)
L/R-Au_{20}（α CD）	3.5×10^{-3}(9)	$Au_{40}(2\text{-}PET)_{24-x}(CamS)_x$	6×10^{-5}(19)
$Ag_{78}(R/S\text{-}BDPP)_6(SR)_{42}$	2×10^{-3}(10)	$Au_{40}(2\text{-}PET)_{24-x}(S\text{-}BINAS)_x$	7.5×10^{-4}(19)
$Au_{38}(2\text{-}PET)_{24}$	4×10^{-3}(11)	$Au_{40}(2\text{-}PET)_{24}$	6×10^{-3}(20)

Table S2 Crystal data and structure refinement for R-Au_{19} and S-Au_{19}.

CCDC Number	2381009	2381011
Identification code	R-Au_{19}	S-Au_{19}
Empirical formula	$C_{155.5}H_{244}Au_{19}ClP_2S_{13}$	$C_{155.5}H_{244}Au_{19}ClP_2S_{13}$
Formula weight	6370.03	6370.03
Temperature/K	120	120.15
Crystal system	orthorhombic	orthorhombic
Space group	$P2_12_12_1$	$P2_12_12_1$
a/Å	19.1670(3)	19.2020(3)
b/Å	22.9143(6)	22.8560(4)
c/Å	43.0420(7)	43.0315(7)
α/°	90	90
β/°	90	90
γ/°	90	90
Volume/Å^3	18904.0(7)	18885.7(5)
Z	4	4
ρ_{calc}g/cm^3	2.238	2.240
μ/mm^{-1}	28.858	28.886
F(000)	11732.0	11732.0
Crystal size/mm^3	0.8 × 0.2 × 0.05	0.265× 0.088 × 0.017
Radiation	Cu Kα (λ = 1.54184)	Cu Kα (λ = 1.54184)
2Θ range for data collection/°	4.106 to 135.982	4.378 to 156.816
Index ranges	-9 ≤ h ≤ 23, -26 ≤ k ≤ 27, -44 ≤ l ≤ 51	-24 ≤ h ≤ 23, -27 ≤ k ≤ 29, -45 ≤ l ≤ 54
Reflections collected	63965	120403
Independent reflections	31355 [R_{int} = 0.1334, R_{sigma} = 0.1339]	38612[R_{int} = 0.1054, R_{sigma} = 0.0803]
Data/restraints/parameters	31355/2644/1687	38612/2105/1736
Goodness-of-fit on F^2	1.140	1.091
Final R indexes [I>=2σ (I)]	R_1 = 0.1239, wR_2 = 0.3041	R_1 = 0.0688, wR_2 = 0.1844
Final R indexes [all data]	R_1 = 0.1479, wR_2 = 0.3288	R_1 = 0.0961, wR_2 = 0.2012
Largest diff. peak/hole / e Å^{-3}	5.26/-3.40	3.16/-2.35
Flack parameter	0.03(3)	0.11(2)

References

(1) G. Deng, S. Malola, J. Yan, Y. Han, P. Yuan, C. Zhao, X. Yuan, S. Lin, Z. Tang, B. K. Teo, H. Häkkinen and N. Zheng, From Symmetry Breaking to Unraveling the Origin of the Chirality of Ligated $Au_{13}Cu_2$ Nanoclusters, *Angew. Chem. Int. Ed.*, 2018, **57**, 3421-3425.

(2) J. Yan, H. Su, H. Yang, C. Hu, S. Malola, S. Lin, B. K. Teo, H. Häkkinen and N. Zheng, Asymmetric synthesis of chiral bimetallic $[Ag_{28}Cu_{12}(SR)_{24}]^{4-}$ nanoclusters via ion pairing, *J. Am. Chem. Soc*., 2016, **138**, 12751-12754.

(3) Y. Yang, Q. Zhang, Z. Guan, Z. Nan, J. Wang, T. Jia and W. Zhan, Enantioselective synthesis of homochiral Au_{13} nanoclusters and their chiroptical activities, *Inorg. Chem.*, 2019, **58**, 3670-3675.

(4) W.-D. Liu, J.-Q. Wang, S.-F. Yuan, X. Chen and Q.-M. Wang, Chiral superatomic nanoclusters Ag_{47} induced by the ligation of amino acids, *Angew. Chem. Int. Ed.*, 2021, **60,** 11430-11435.

(5) H. Shen, Z. Xu, L. Wang, Y.-Z. Han, X. Liu, S. Malola, B. K. Teo, H. Häkkinen and N. Zheng, Tertiary chiral nanostructures from C-H···F directed assembly of chiroptical superatoms, *Angew. Chem. Int. Ed.*, 2021, **60**, 22411-22416.

(6) W. Du, X. Kang, S. Jin, D. Liu, S. Wang and M. Zhu, Different types of ligand exchange induced by Au substitution in a maintained nanocluster template, *Inorg. Chem.*, 2020, **59**, 1675-1681.

(7) J. Zhou, T. Li, Q. Li, P. Zheng, S. Yang, J. Chai and M. Zhu, Insight into the effects of chiral diphosphine ligands on the structure and optical properties of the $Au_{24}Cd_2$ nanocluster, *Inorg. Chem.*, 2022, **61**, 6493-6499.

(8) J.-Q. Wang, Z.-J. Guan, W.-D. Liu, Y. Yang and Q.-M. Wang, Chiroptical Activity Enhancement via Structural Control: The Chiral Synthesis and Reversible Interconversion of Two Intrinsically Chiral Gold Nanoclusters, *J. Am. Chem. Soc.*, 2019, **141**, 2384-2390.

(9) Y. Zhu, H. Wang, K. Wan, J. Guo, C. He, Y. Yu, L. Zhao, Y. Zhang, J. Lv, L. Shi, R. Jin, X. Zhang, X. Shi and Z. Tang, Enantioseparation of $Au_{20}(PP_3)_4Cl_4$ Clusters with Intrinsically Chiral Cores, *Angew. Chem. Int. Ed.*, 2018, **57**, 9059.

(10) H. Yang, J. Yan, Y. Wang, G. Deng, H. Su, X. Zhao, C. Xu, B. K. Teo and N. Zheng, From Racemic Metal Nanoparticles to Optically Pure Enantiomers in One Pot*, J. Am. Chem. Soc.*, 2017, **139**, 16113-16116.

(11) I. Dolamic, S. Knoppe, A. Dass and T. Bürgi, First enantioseparation and circular dichroism spectra of Au_{38} clusters protected by achiral ligands, *Nat. Commun.*, 2012, **3**, 798.

(12) Y. Yanagimoto, Y. Negishi, H. Fujihara and T. Tsukuda, Chiroptical Activity of BINAP-Stabilized Undecagold Clusters, *J. Phys. Chem. B,* 2006, **110**, 11611–11614.

(13) M. Sugiuchi, Y. Shichibu and K. Konishi, An Inherently Chiral Au_{24} Framework with Double-Helical Hexagold Strands, *Angew. Chem. Int. Ed.*, 2018, **57**, 7855.

(14) T. Nakashima, R. Tanibe, H. Yoshida, M. Ehara, M. Kuzuhara and T. Kawai, Self-Regulated Pathway-Dependent Chirality Control of Silver Nanoclusters, *Angew.*

Chem. Int. Ed., 2022, **61**, e202208273.

(15) W.-D. Si, Y.-Z. Li, S.-S. Zhang, S. Wang, L. Feng, Z.-Y. Gao, C.-H. Tung and D. Sun, Toward Controlled Syntheses of Diphosphine-Protected Homochiral Gold Nanoclusters through Precursor Engineering, *ACS Nano*, 2021, **15,** 16019-16029.

(16) C. Liu, Y. Zhao, T.-S. Zhang, C.-B. Tao, W. Fei, S. Zhang and M.-B. Li, Asymmetric transformation of achiral gold nanoclusters with negative nonlinear dependence between chiroptical activity and enantiomeric excess, *Nat. Commun.*, 2023, **14**, 3730.

(17) J. Olesiak-Banska, M. Waszkielewicz, P. Obstarczyk and M. Samoc, Two-photon chiro-optical properties of gold Au_{25} nanoclusters, *Chem. Soc. Rev.*, 2019, **48**, 4087.

(18) Q. Xu , S. Kumar , S. Jin , H. Qian , M. Zhu and R. Jin, Chiral 38-Gold-Atom Nanoclusters: Synthesis and Chiroptical Properties, *Small*, 2014, **10**, 1008-1014.

(19) S. Knoppe, A. Dassb and T. Bürgi, Strong non-linear effects in the chiroptical properties of the ligand-exchanged Au_{38} and Au_{40} clusters, *Nanoscale*, 2012,**4**, 4211-4216.

(20) S. Knoppe, I. Dolamic, A. Dass, and T. Bürgi, Separation of Enantiomers and CD Spectra of $Au_{40}(SCH_2CH_2Ph)_{24}$:Spectroscopic Evidence for Intrinsic Chirality, *Angew. Chem. Int. Ed.*, 2012, **51**, 7589-7591.